ATOMIC ELECTRONS SHAKE-OFF ACCOMPANYING ALPHA DECAY

Contents

ATOMIC ELECTRONS SHAKE-OFF ACCOMPANYING ALPHA DECAY

Meir Shimshon Rapaport

Lawrence Berkeley Laboratory
University of California
Berkeley, California 94720

ABSTRACT

The α spectra associated with K-shell electron shake-off in ^{210}Po and ^{238}Pu decay have been determined by K x-ray - α coincidence measurements. Although the shapes of the spectra generally agree with theoretical expectations, some discrepancies are observed. From similar measurements the α spectra associated with L and M - shell electrons shake-off in ^{210}Po were determined. The abundances per α particle of the total K, L and M electron shake-off effects were determined in these measurements and found to be $P_K = (1.65\pm0.16) \times 10^{-6}$, $P_L = (7.23\pm0.65) \times 10^{-4}$ and $P_M = (1.84\pm0.37) \times 10^{-2}$ for ^{210}Po and $P_K = (0.75\pm0.09) \times 10^{-6}$ for ^{238}Pu. Also, the abundances per α particle of the L subshell electron shake-off effect were found to be $P_{L_1} = (5.11\pm0.40) \times 10^{-4}$, $P_{L_2} = (0.62\pm0.06) \times 10^{-4}$ and $P_{L_3} = (1.50\pm0.19) \times 10^{-4}$. Only limits on the ionizations probabilities of M subshells could be determined. These limits were: $P_{M_2} = 7 - 23\%$, $P_{M_4} < 24\%$, $P_{M_5} < 17\%$ and $P_{M_1} + P_{M_5} > 47\%$ of the total. These results are also compared with theoretical predictions. Further experimental and theoretical studies are suggested.

I. INTRODUCTION

The phenomenon by which an electron in a given orbital is excited into the continuum (shake-off) during nuclear decay was first treated by Migdal[1] and Feinberg[2] and later by Levinger[3] (all are perturbation type calculations). Since then much theoretical[4-10] and experimental[11-17] work related to β^-, β^+ and E.C. decay has been done. The various experimental works involved measurements of x-ray -β coincidences, β and x-ray intensities, relative x-ray and γ-ray intensities and relative intensities of x-rays in parent and daughter nuclei. Shake-off of L electrons accompanying internal conversion in the K-shell was also observed.[18] The agreement between theory and experiment has in general been good. Recently, a distinctly different type of theoretical treatment of the shake-off phenomenon accompanying α decay was published by Hansen.[19]

Essentially, all of the measurements[20-27] of electron shake-off during α decay have been made on ^{210}Po with one unpublished result on ^{238}Pu. In the ^{210}Po experiments the x-ray abundances were measured and any excess over that expected from the internal conversion of the 803 KeV γ-ray was assumed to be due to electron shake-off. The measurement[28] of the K-shell effect in ^{238}Pu decay was very similar, but more involved because of additional gamma rays.

The K-shell effect was studied[20-23] by measuring the radiation of ^{210}Po using proportional counters or NaI scintillation counters and the radiation was easily established to be lead K x-rays. The agreement between experiment and perturbation type theory has not been good. Gener-

ally, the experimental results for the K shell probability were about 60% of the theoretical predictions, and the discrepancy was about twice the stated experimental error. On the other hand, Hansen's theoretical predictions of K shell ionization are in good agreement with experiment.

Several measurements of the total shake-off phenomenon in the L and M shell exist. Curie and Joliot[24] were the first to observe the soft radiation associated with alpha decay of ^{210}Po. They detected the photons by means of an ionization chamber connected to an electroscope and identified photon energies by absorption coefficients. They believed the radiation to be Po x-rays excited by α particles. However, they stated that their technique could not distinguish between lead and polonium photons. Riou[25] identified the L x-rays associated with ^{210}Po alpha decay as lead x-rays. He used a Geiger-Müller detector and identified the soft radiation by selective absorption coefficients. Rubinson and Bernstein[26] and later Rubinson[27] studied the L and M x-rays respectively. They used a proportional counter and were able to observe some of the structure associated with filling the vacancies in the L and M shells. The discrepancy between experiments and perturbation type theory is very large. Again, Hansen's theoretical predictions are in good agreement with experiment.

A different kind of experimental evidence of the shake-off phenomenon is the charge distribution of the recoiling daughter atoms after alpha decay. The charge distributions of several alpha emitters were studied[29-33] and they varied from -1 to +10 in the absence of internal conversion.

Approximately 90% of the recoiling atoms carried zero or +1 charge and the mean charge was less than 1. However, these charge distributions were due mostly to outer shell electron ionization rather than K, L and M shells.

The present work (with high resolution solid state detectors) was undertaken to measure directly that part of the alpha spectrum connected with the electron shake-off effect in the K (^{210}Po and ^{238}Pu sources) and the L and M (^{210}Po source) shells. In the same time the differential shape of this spectrum was to be determined and the results compared with theoretical predictions. Also, the initial L subshell vacancies and the yields of K and M x-rays that result from the shake-off effect were to be determined.

II. EXPERIMENTAL WORK

The general experimental procedure was to measure the energy and abundances of the alpha spectrum which was in coincidence with K, L and M x-rays as well as the energies and abundances of the L and M x-rays. Two alpha emitters, ^{210}Po and ^{238}Pu, were studied. The shake-off effect in the K, L and M shells was studied in ^{210}Po while the shake-off effect accompanying the α decay of ^{238}Pu was studied only in the K shell.

Two different experimental systems were used. One system was utilized to measure the K shell effect and the second system was utilized to measure the shake-off effect in the L and M shells. The two systems are described in the following sections.

The coincidence systems were assembled with the following objectives in mind: (1) obtain the largest geometry factor possible for the x-ray detectors; (2) reduce the background radiation detected by the x-ray detectors as much as possible to make the rate of accidental coincidences acceptable; and (3) maintain adequate α detector resolution in spite of the intense α radiation.

A. Alpha - K X-Ray Coincidence Measurement

1. Equipment

a. Vacuum Chamber

The x-ray detector housing was positioned at one end of a cylindrical aluminum vacuum chamber 3.5 inches long and 2.0 inches inside diameter. The α detector housing penetrated the vacuum chamber from the

opposite side. The position of the α detector was mechanically controlled from outside the vacuum chamber and the α detector could be positioned anywhere between the two ends of the vacuum chamber. The source to be studied was mounted on a thin lucite ring which was then attached to the face of the x-ray detector housing. Thus, the source-to-detector distance was variable for the α side but not for the x-ray side. When a coincidence experiment was not in progress, a mechanically controlled aluminum foil could be placed between the source and the α detector to protect the latter from the intense α radiation.

An oil pump was used to evacuate the vacuum chamber. A cold trap (dry ice + alcohol) was connected to the pumping line to prevent the oil from coating the α detector.

b. K X-Ray Side

The K x-rays were detected with a solid state detector of pure Ge which had a thin aluminum window. The detector had a full-width-at-half-maximum (F-W-H-M) of 1.0 KeV for a 122 KeV γ-ray and an overall detection efficiency of 13.5% at that energy. To determine the efficiency curve, γ rays in standard efficiency sources of known disintegration rates were measured. The standard sources were: ^{241}Am, ^{203}Hg, ^{57}Co, ^{22}Na, ^{137}Cs and ^{54}Mn.

The detector's output was amplified and fed into a singel channel analyzer (see Fig. 1). In the ^{210}Po measurement, this alayzer was set on the K_α x-rays, which comprise 78% of the total. Figure 2 shows the photon radiation between 20 KeV and 150 KeV. The marked area shows the

energy region that the single channel analyzer was set on. In the ^{238}Pu measurement, however, the single channel analyzer was set on the K_β x-rays, which are only 23%[34] of the total K x-rays, in order to eliminate the α spectrum in coincidence with the 100 KeV γ-ray. Figure 3 shows the photon radiation between 35 KeV and 180 KeV. Again, the marked area shows the energy region that the single channel analyzer was set on. In this latter experiment the γ-ray output of the preamplifier was gain-stabilized. The output of the single channel analyzer was part of a fast-slow triple coincidence system. The block diagram is shown in Fig. 1.

c. α Side

The α particles were detected with Au-Si surface barrier type detectors (12 mm in diameter) with geometries of about 2-3%. The intense bombardment of the detector by the α activity of the sources resulted in a deterioration of resolution over the course of the experiments. In the ^{210}Po measurement the F-W-H-M changed from 22.5 KeV at the beginning of the experiment to 30.0 KeV at the end. For the ^{238}Pu measurement the F-W-H-M changed from 30.0 to 36.5 KeV.

The α detector output was first sent to a gain-stabilizer. Then part of the output was fed into the triple coincidence system, part was fed into a unit which scaled down the counting rate by a factor of 20 and part was fed to a 400 channel pulse height analyzer through a bias amplifier and a linear gate. The linear gate was triggered via a mixer gate by either pulses from the triple coincidence system or the scaled-

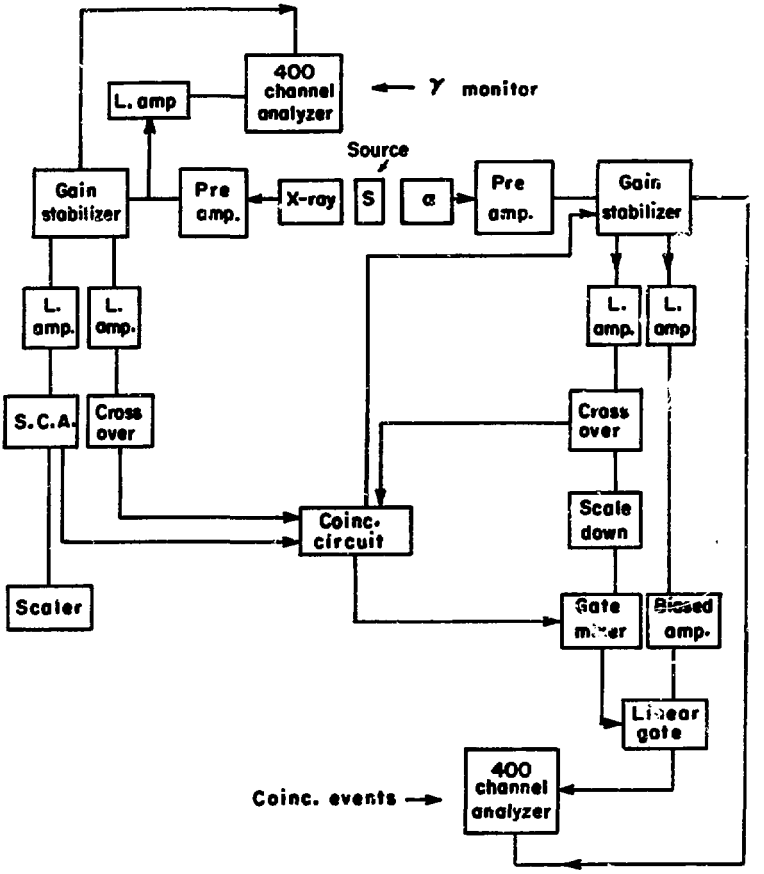

XBL744-2822

Fig. 1

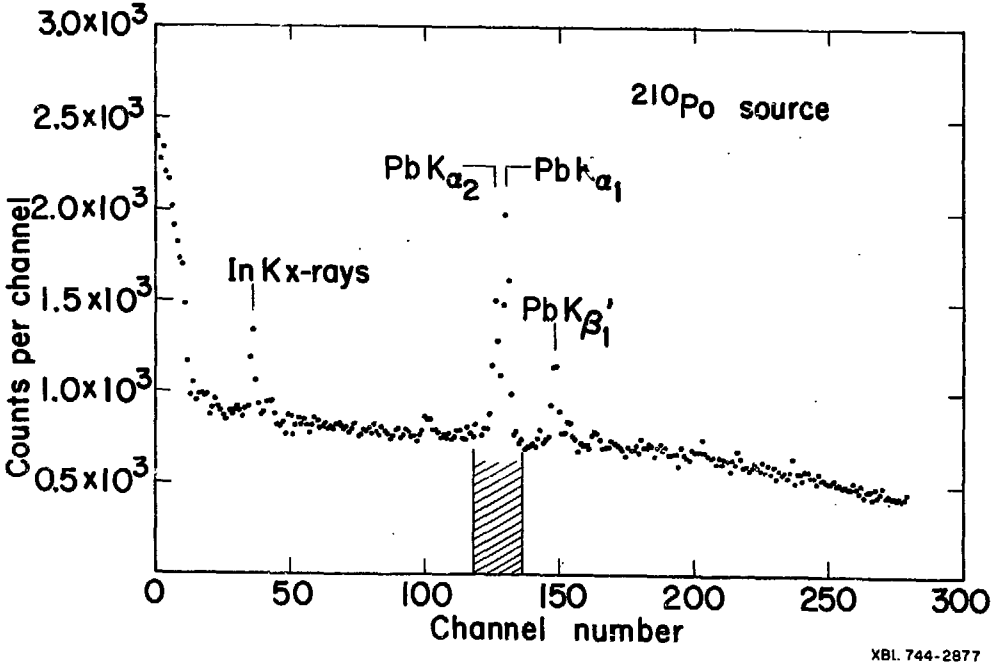
3.0x10^3
2.5x10^3
2.0x10^3
1.5x10^3
1.0x10^3
0.5x10^3
Counts per channel
210Po source
Pb Kα2
Pb Kα1
In K x-rays
Pb Kβ1'
0
50
100
150
200
250
300
Channel number
XBL 744-2877

Fig. 2

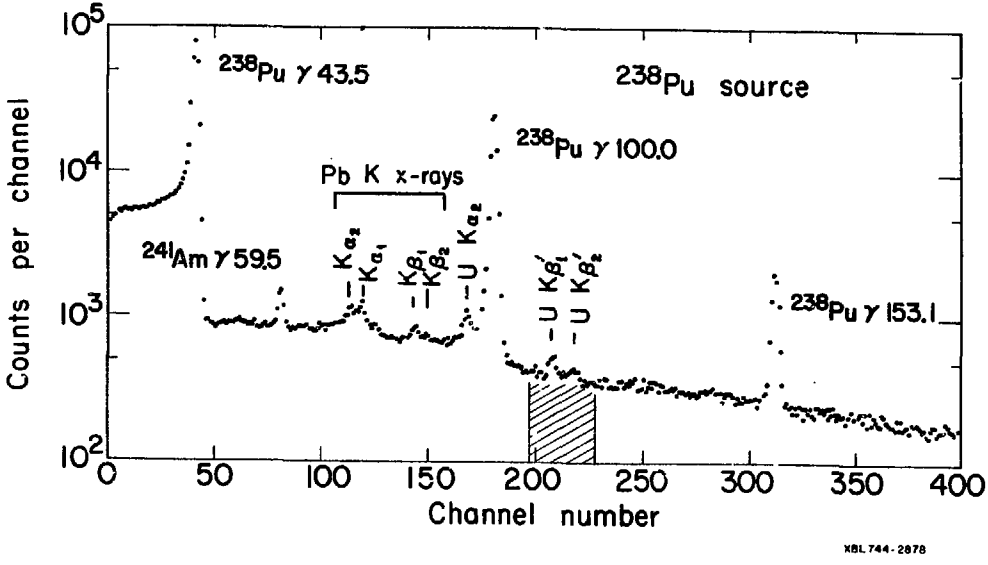
Counts per channel
Channel number
238Pu γ 43.5
238Pu source
238Pu γ 100.0
Pb K x-rays
241Am γ 59.5
Kα2
Kα1
Kβ1
Kβ2
U Kα2
U Kβ1'
U Kβ2'
238Pu γ 153.1
XBL 744-2878

Fig. 3

down α singles pulses. The pulse height analyzer was also gated by the triple coincidence system via the gain-stabilizer so that only coincidence pulses were stored and not the scaled-down singles used for gain stabilization.

The net effect of the electronic arrangement was that α pulses which were in coincidence with the K x-ray gate could register on the pulse height analyzer with a minimum of accidental coincidences (72×10^{-9} sec resolving time) and without any gain change during the experiment.

The whole system was enclosed in walls made of lead bricks. These served to reduce the background radiation detected by the x-ray detector and hence reduced the probability of accidental coincidences. When the Po source was studied additional steel bricks and aluminum plates were placed against the lead brick walls. They prevented any lead x-rays excited in the lead bricks from reaching the x-ray detector.

2. Source Preparation

The ^{238}Pu was chemically purified by dissolving in 12 M HCl, loading onto an anion column (DOWEX AG 1x8%), washing the column with 12 M HCl containing some HNO_3 and eluting the ^{238}Pu off the column with a solution of 12 M in HCl and .44 M in HI. The eluent was evaporated to dryness and then vaporized in vacuum from a tungsten filament onto a .002 inch thick mylar foil. The source which had been collimated to an area 5/16 inch in diameter during vaporization was invisible and had an activity of $\sim 1.2 \times 10^7$ α dis/min.

The ^{238}Pu source was of high purity as is indicated in Fig. 3.

But for the γ rays associated with the decay of ^{238}Pu, uranium x-rays were observed. They originated from the internal conversion of the 153.1 KeV γ-rays and the shake-off phenomenon. In addition, the 59.5 KeV γ-rays associated with the decay of ^{241}Am were observed. Part of the latter activity was due to ^{241}Am impurity in the source and part was due to ^{241}Am activity that scattered in the vacuum chamber during the calibration of the system. Also observed were lead K x-rays which were excited in the lead brick wall that surrounded the whole system and then detected in the x-ray detector.

Two vials of ^{210}Po were purchased from New England Nuclear. The ^{210}Po was catalogued as carrier-free and of natural origin although investigation at the conclusion of the experiment showed it was prepared by the reaction and decay: $^{209}Bi\ (n,\gamma)\ ^{210}Bi \xrightarrow[5\ day]{\beta^-} {}^{210}Po$. The ^{210}Po from one of the vials was further purified by fuming to near dryness with concentrated HNO_3 loading onto a cation column (DOWEX 50) with .2 M HCl, washing with 2 M HNO_3 and eluting the ^{210}Po with 2 M HCl. The overall yield of the above procedure was ∿ 20%. The eluent was evaporated to dryness and vaporized like the ^{238}Pu onto a .002 inch thick mylar foil. The source was ∿ 1.7×10^7 α dis/min and was invisible.

The ^{210}Po source was very pure as is indicated in Fig. 2. Except for lead x-rays only indium K x-rays were observed. The latter originated from the indium foil which was part of the x-ray detector.

B. Alpha - L and M X-Ray Coincidence Measurement

1. Equipment

a. Vacuum Chamber

The x-ray detector housing was positioned at about the center of a cubic (5.5 inch in dimension) aluminum vacuum chamber. The housing had a .001 inch thick beryllium window which could be opened once a good vacuum was established in the chamber. A motor driven α detector penetrated the vacuum chamber from the side opposite the x-ray detector. The sources to be studied were mounted on the α detector housing about 1 cm away from the α crystal and could be brought within 3 mm of the face of the x-ray crystal. The source-to-detector distance was variable for the x-ray side but not for the α side. When a coincidence experiment was not in progress, a magnetically controlled nickel foil could be placed between the source and the α detector to protect the latter from the intense α radiation.

A cyrogenic pump, two 8 liter ion pumps and a cold finger were used to evacuate the vacuum chamber. On the average 6 hours of pumping were needed before a pressure of $\sim 10^{-7}$ mm of Hg was reached and the beryllium window on the face of the x-ray detector housing could be opened.

b. X-Ray Side

The x-rays were detected with a Si(Li) solid state detector which was 5 mm in diameter and 3 mm thick. The detector had a full-width-at-half-maximum (F-W-H-M) of 180 eV for 6.46 KeV iron K x-rays.

In the experimental arrangement the maximum overall detection efficiency (which includes the geometry of the system) was 6.0% for 10 KeV radiation and at 3.3 KeV this was reduced to 2.55%.

To determine these efficiencies ^{241}Am, ^{57}Co, ^{65}Zn and ^{54}Mn were separately vaporized in vacuum from tungsten filaments onto .001 inch thick beryllium disks. The sources were collimated to an area 2 mm in diameter during vaporization. The absolute disintegration rate of the sources were determined by measuring the abundances of their γ-rays and comparing them with known standards of the same isotopes. Tabulated[35-37] values of the intensities of x-rays and low energy γ-rays associated with the above sources were then used to determine the x-ray detector efficiency curve.

The preamplifier utilized a low-noise field-effect transistor at low temperature with pulsed optical feedback. Final amplification was accomplished by an Amplifier System Module[38] which contained a linear amplifier (17 μ sec time constant), a biased amplifier and a pile-up rejector. The output was fed both into a coincidence circuit and into an analog-to-digital converter (A.D.C.) which fed a two parameter coincidence system. The block diagram for the system is shown in Fig. 4. The linearity of the amplifier-analyzer system for x-rays was better than .3% and no shift in energy was observed in the 5 months of experiments.

c. α Side

The α particles were detected with a Au-Si surface-barrier type

crystal (6 mm in diameter) with a geometry of .80% and resolution of 20.0 KeV (F-W-H-M). The α detector was operated at 4°C, and no deterioration of its resolution was observed during the experiments although the pulse amplitude gradually decreased with time. The energy linearity of the amplifier-analyzer system for α particles was better than .5% in the region of interest.

The α detector output was amplified and then fed both into the coincidence circuit and into a separate A.D.C. The output from this A.D.C. was fed into a gain stabilizer, which operated only on those pulses that were in coincidence with x-ray pulses. After 8 days of operation the gain stabilizer was not able to compensate for the decreasing preamplifier output and the pulse height out of the amplifier also began gradually decreasing. The pulses from both the x-ray side and α side A.D.C.'s were routed into a two parameter coincidence system as shown in Fig. 4. The data was reduced with the computer program MULTI[39].

2. Source Preparation

The ^{210}Po was of the same origin as the ^{210}Po used in the K shell measurements. In addition to the ^{210}Po 803 KeV γ-ray, low intensity Ba K x-rays were observed as well as the ^{210}Pb 47 KeV γ-ray. Since the above radiations do not interfere with the experiments the ^{210}Po was not further purified.

The ^{210}Po activity was vaporized in vacuum from a tungsten filament onto a .001 inch thick beryllium disk in exactly the same way

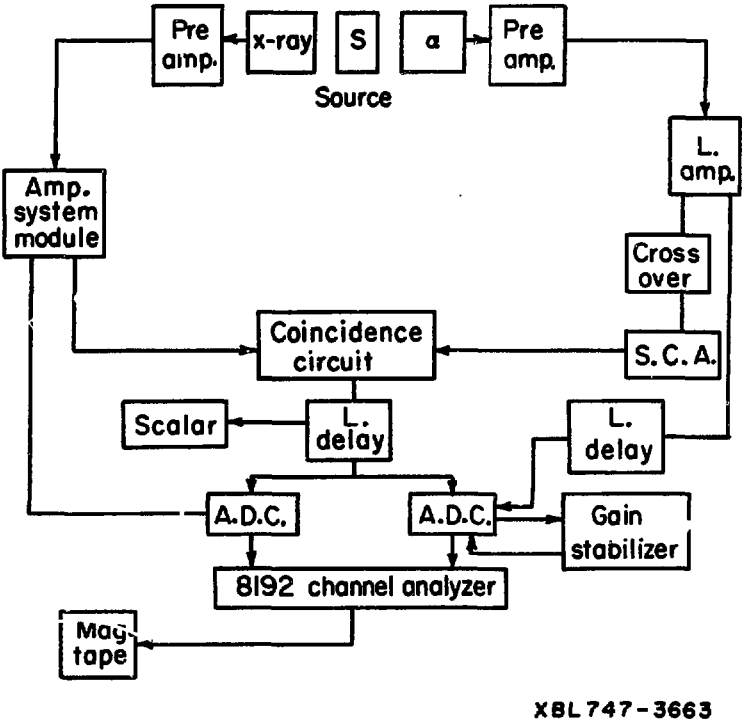
Pre amp.
x-ray
S
α
Pre amp.
Source
L. amp.
Amp. system module
Cross over
Coincidence circuit
S.C.A.
Scalar
L. delay
L. delay
A.D.C.
A.D.C.
Gain stabilizer
8192 channel analyzer
Mag tape
XBL747-3663

Fig. 4

as in the efficiency determinations. The latter was thick enough to stop any of the α particles from reaching the x-ray detector. The source, which had been collimated to an area 2 mm in diameter during vaporization, had an activity of $\sim$ 2.6 x 10^6 α dis/min.

III. RESULTS

A. K Shell Shake-off

1. ^{238}Pu

The ^{238}Pu was measured in the coincidence unit for a total running time of 15 days. The singles spectra were measured and recorded every day as were the coincident spectra. The γ singles spectra were monitored continuously. The α - K x-ray coindicnece spectra for the one day runs were summed and this total spectrum is presented in Fig. 5. The abscissa is the analyzer channel in which the coincidences appeared, and it is roughly linear with the α particle energy. The ordinate is the total number of observed coincidences in the 15 days period. The highest energy peaks, α_o and α_{44}, are due to accidental coincidences between the most intense α groups and radiation in the K x-ray gate. The most intense peak, α_{296}, is due to true coincidences with K x-rays from conversion of the 153 KeV γ-ray and with the Compton background of this γ-ray in the K x-ray gate region. The pertinent part of the ^{238}Pu decay scheme is shown in Fig. 6.

The α_{296} coincident peak (see Fig. 5) is broader than the α_o and α_{44} accidental peaks and this is probably due to a combination of effects including shifts in the threshold of the bias amplifier and a non-linearity in this region of the pulse height analyzer. The broad α distribution (see Fig. 5) in the region of channels 175-260 is broader than α_{296}, tails substantially more on the low energy side and, if the shake-off effect is excluded, would not correspond to any α groups of

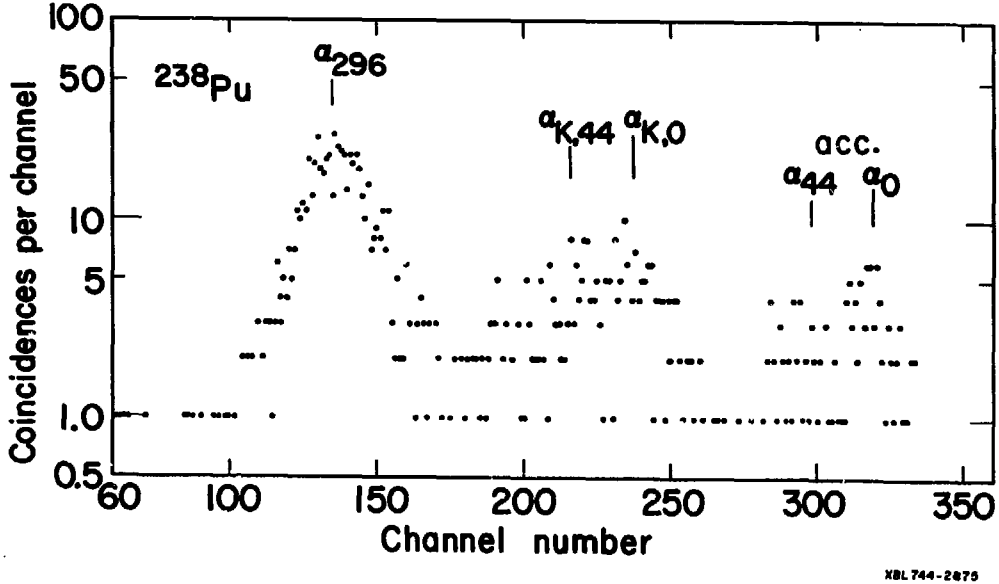
100
50
10
5
1.0
0.5
Coincidences per channel
238Pu
α296
αK,44
αK,0
acc.
α44
α0
60
100
150
200
250
300
350
Channel number
XBL 744-2875

Fig. 5

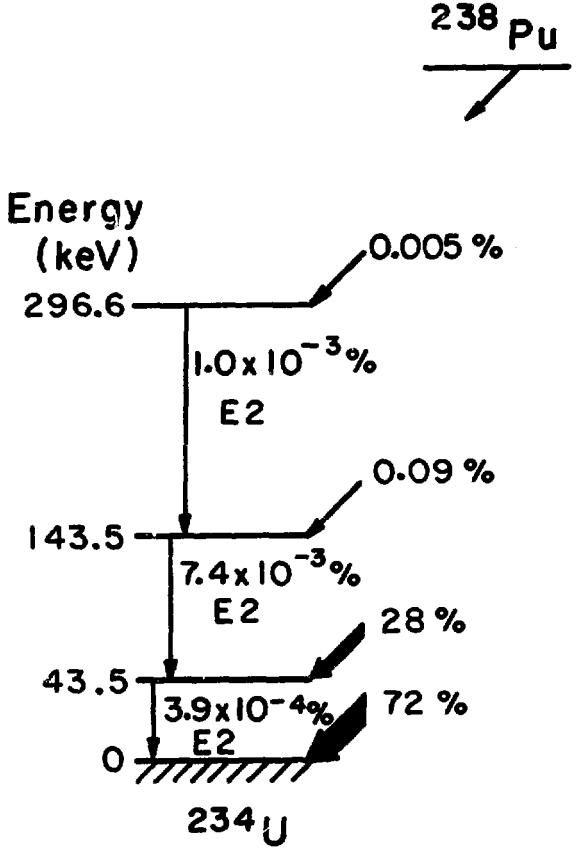

XBL744-2823

Fig. 6

^{238}Pu expected to be in coincidence with the K_β x-ray gate. A measurement was made of the maximum amount of the 100 KeV γ-gate of ^{238}Pu which could be in the gate region. It indicated that only a negligible proportion of the coincidences in the region of channels 175-260, could be due to this γ-ray. To determine if these observed coincidences had the proper maximum energy for a ^{238}Pu α_o particle which ejected a K electron with about zero kinetic energy their high energy side (see Fig. 5) and that of ^{238}Pu α_o was extrapolated to $\sim$ 1/4 of their peak height. There was a difference in energy of 115 ± 10 KeV which agrees with the K binding energy of uranium, 115.6 KeV.

Thus, the distribution in Fig. 5 in the region of channel 175-260 should be due to the electron shake-off effect of the main alpha groups. The distribution is spread out over so many channels because there are two major α groups involved, α_o and α_{44}, and because the shake-off electrons carry off energy causing a spread in α particle energy and a tailing on the low energy side. There was a total of 271 coincidences ($\sim$ 264 and $\sim$ 7 accidentals) measured in the 15 day experiment in the region of interest (channel 175-260). From the true coincidence counting rate, the α singles counting rate, the K x-ray side detector efficiency (including geometry), the fraction of total K x-rays in the gate and the K shell fluorescence yield, the abundance of ejected K shell electrons is (0.75 ± 0.09) x 10^{-6} per ^{238}Pu α particle.

The nomenclature for the normal α groups shown in Fig. 5 is the usual one with the energy of the excited state being a subscript to the

α symbol, e.g., the ^{238}Pu α groups populating the 44 KeV excited state in ^{234}U is designated $^{238}Pu\ \alpha_{44}$ or simply α_{44}. I suggest for the α groups ejecting orbital electrons in their passage through the coulomb field, that the shell designation of the ejected electrons be added as a subscript before the excited state energy. Thus, the ^{238}Pu α group which populates the 44 KeV state in ^{234}U and which also causes a K electron to be ejected would be designated $^{238}Pu\ \alpha_{K,44}$ or simply $\alpha_{K,44}$.

2. ^{210}Po

The ^{210}Po was also measured in the coincidence unit for a total running time of 15 days. The experiment was very similar to that for ^{238}Pu except that a larger fraction of the K x-ray peak could be used in the gate as there are no gamma rays in ^{210}Po decay near the gate energy. The various coincidence runs in the 15 day period were summed and the total spectrum is shown in Fig. 7. The highest energy peak, α_o, is due to accidental coincidences with the main α group. The only other known α group of ^{210}Po populates the 803 KeV excited state of ^{206}Pb and has a very low abundance[40] of 1.07×10^{-5}. The peak at ~ channel 340 (see Fig. 7) is broader than α_o and tails more on the low energy side.

The linearity of the amplifier-analyzer system for particles was carefully checked with ^{240}Pu and ^{242}Pu and was found to be linear within 1% in the region of interest. Thus, the increased peak width is not due to non-linearity in the energy scale and is very likely caused by the kinetic energy carried off by the K electrons ejected during the

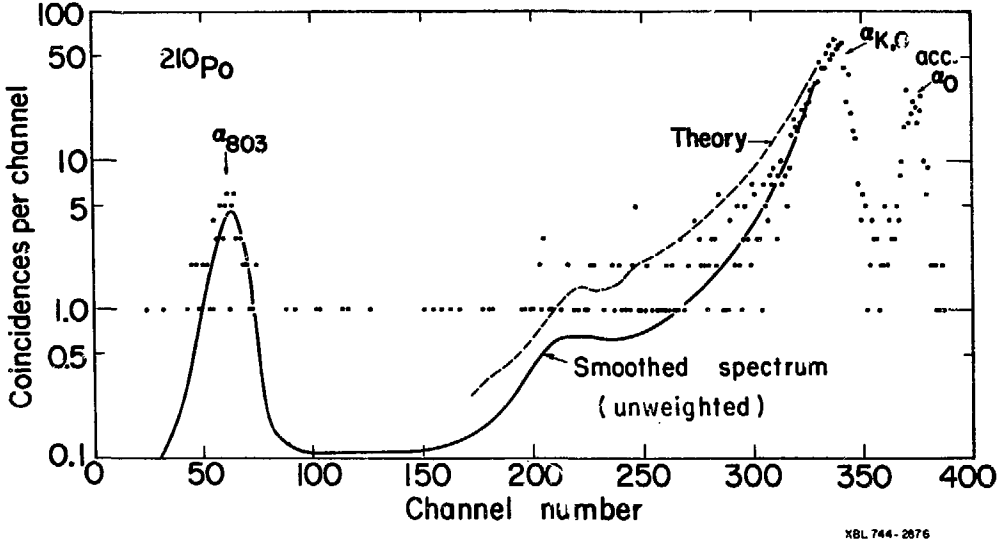
100
50
10
5
1.0
0.5
0.1
Coincidences per channel
210Po
α803
αK,0
acc.
α0
Theory
Smoothed spectrum
(unweighted)
0
50
100
150
200
250
300
350
400
Channel number
XBL 744-2876

Fig. 7

α decay process as in ^{238}Pu decay. By extrapolating the two peaks (see Fig. 7) in the same fashion as for the ^{238}Pu experiment, a difference in energy of 88 ± 1 KeV was found in excellent agreement with K shell binding energy of lead, 88.0 KeV.

There was a total of 1,347 coincidences (∿ 1,285 true and ∿ 62 accidental) in the region of the α shake-off peak, $^{210}Po\ \alpha_{K,0}$. Calculated in the same way as for the ^{238}Pu experiment the abundance of ejected K shell electrons is (1.65 ± .16) x 10^{-6} per ^{210}Po α particle. As a check on the correctness of the geometry calibration, the K conversion coefficient of α_{803} was calculated from its abundance in the coincidence run (see Fig. 7) and the tabulated singles abundance, 1.07 x 10^{-5}. The resulting value (8.1 ± 1.4) x 10^{-3} is in good agreement with the theoretical[41] E2 K conversion coefficient, 8.08 x 10^{-3}.

B. L and M Shells Shake-Off

The ^{210}Po source was measured in the coincidence unit for a total of 13.3 days during the 14 day experiment. The α singles spectra were measured and recorded on magnetic tape every day as were the coincidence spectra. The spectrum of L x-rays in coincidence with α particles is shown in Fig. 8. In Fig. 9 are shown the coincident M x-rays for the same measurement. A 2.9 day x-ray singles measurement was also made, and the M x-ray region is shown in Fig. 10. The intensities of the L_α peaks in the singles and coincidence runs agreed within 2% which indicated the coincidence efficiency was close to 100%. The α spectra in coincidence with L x-rays and M x-rays are shown in Fig. 11(a-e) for

8 days of measurement.

1. L X-Rays

Figure 8 shows the photon radiation between 9.3 KeV and 18.3 KeV in coincidence with ^{210}Po α particles. Characteristic lead L x-rays are observed as well as impurity x-rays from ^{241}Am near the detector. The L_α peak arises from L_3 vacancy filling, the L_β peaks arise from all three subshells and the L_γ peaks arise from L_1 and L_2 subshells. A spectroscopic diagram of the radiative transitions that comprise the characteristic lead L x-rays is given in Fig. 12.

From the total number of coincidences in a given peak shown in Fig. 8 and the x-ray detector efficiency curve, the following two ratios were found: $P_{L_\alpha}/P_{L_\beta} = 1.14 \pm .06$, $P_{L_\alpha}/P_{L_\gamma} = 5.18 \pm .26$. In addition the ratio $P_{L_\alpha}/P_{L_\ell} = 20.0 \pm 4.0$ was determined from the singles spectrum (not shown since it is similar in shape to the coincidence spectrum but with a larger number of counts registered) because the number of L_ℓ events was too low in the coincidence measurement. P_{L_α}, for example, is the probability per particle of emitting an L x-ray belonging to the L_α peak. From the total number of events in a given peak, the efficiency curve and the α singles counting rate the following abundances were obtained: $P_{L_\alpha} = (1.11 \pm .11) \times 10^{-4}$, $P_{L_\beta} = (9.72 \pm .78) \times 10^{-5}$, $P_{L_\gamma} = (2.15 \pm .32) \times 10^{-5}$, $P_{L_\ell} = (1.11 \pm .22) \times 10^{-6}$. In the above, accidental coincidences and scattered radiation were ignored since their contribution was negligible.

The Probabilities P_{L_α}, P_{L_β}, etc. can be written in terms of P_{L_1},

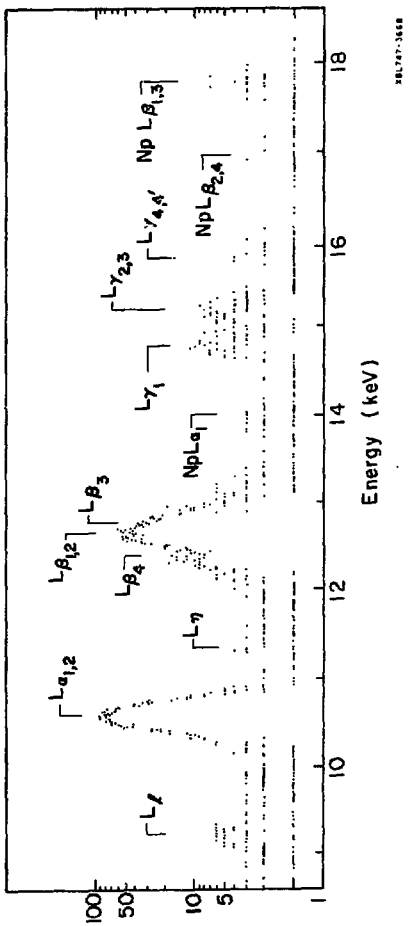
Coincedences per channel
100
50
10
5
1
10
12
14
16
18
Energy (keV)
Lℓ
Lα1,2
Lη
Lβ4
Lβ1,2
Lβ3
NpLα1
Lγ1
Lγ2,3
Lγ4,4'
Np Lβ1,3
NpLβ2,4

Fig. 8

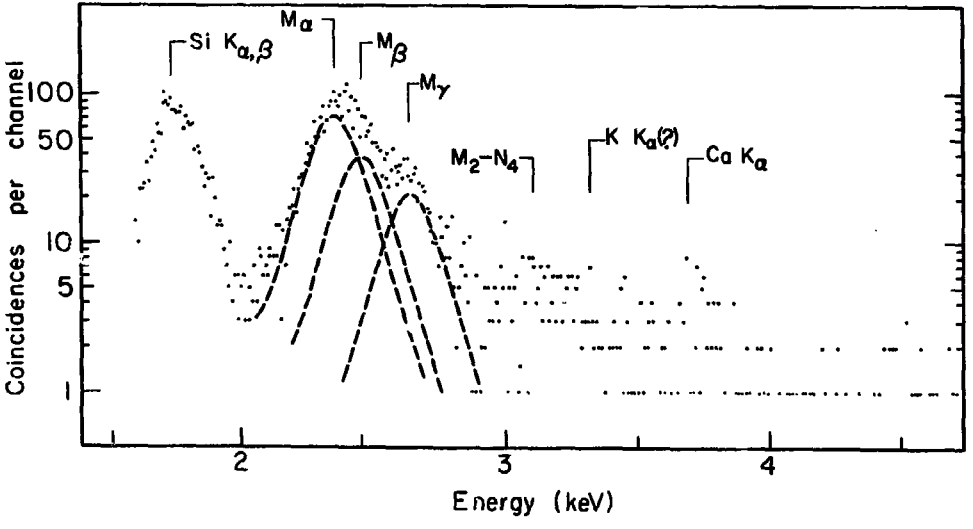

XBL747-3666

Fig. 9

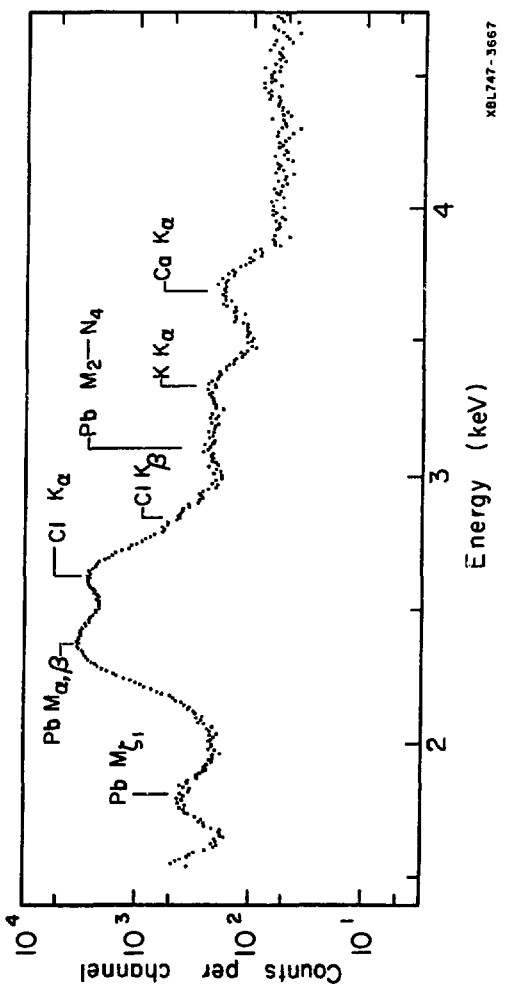
Counts per channel
10^4
10^3
10^2
10^1
Pb $M_{\alpha,\beta}$
Pb M_γ
Cl K_α
Cl K_β
Pb M_2-N_4
K K_α
Ca K_α
2
3
4
Energy (keV)
XBL747-3667

Fig. 10

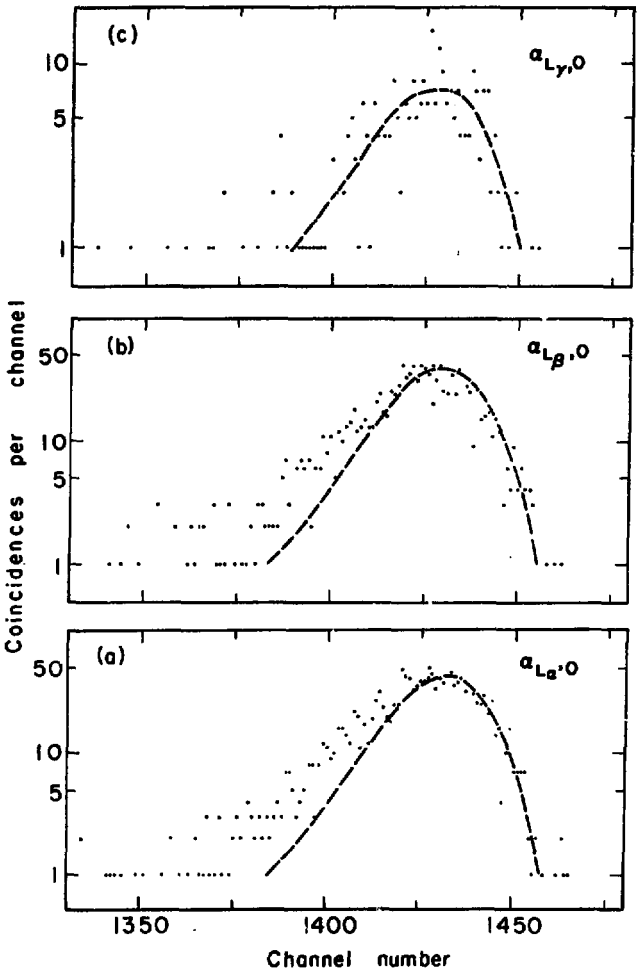
(c)
$\alpha_{L\gamma,0}$
10
5
1
(b)
$\alpha_{L\beta,0}$
50
10
5
1
(a)
$\alpha_{L\alpha,0}$
50
10
5
1
Coincidences per channel
1350
1400
1450
Channel number
XBL747-3669

Fig. 11 (a-c)

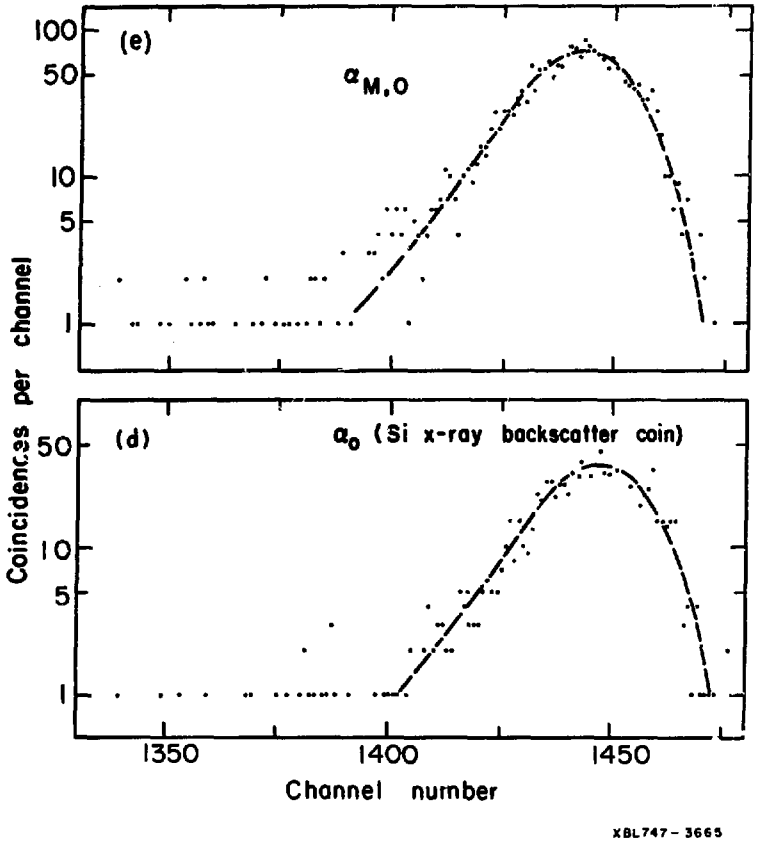
(e)
$\alpha_{M,0}$
100
50
10
5
1
(d)
α_0 (Si x-ray backscatter coin)
50
10
5
1
Coincidences per channel
1350
1400
1450
Channel number
XBL747-3665

Fig. 11 (d,e)

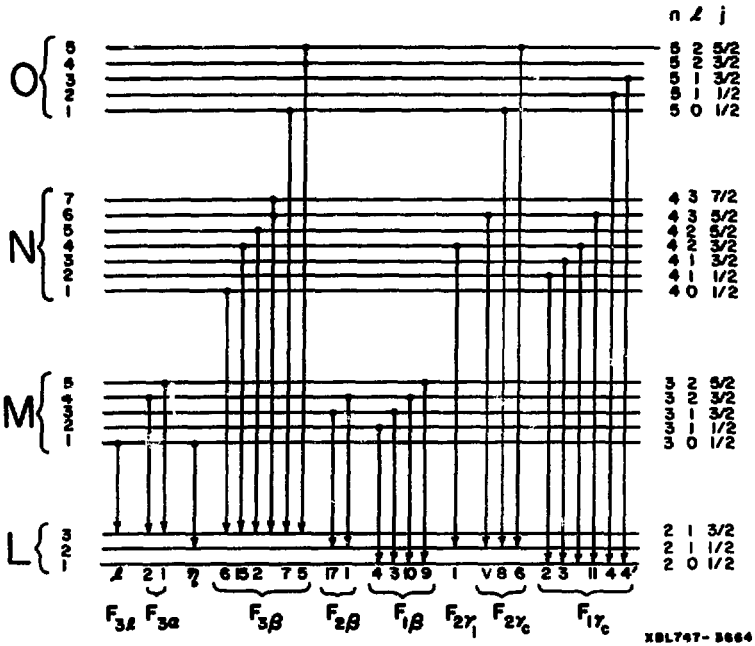
n ℓ j
O
N
M
L
5 2 5/2
5 2 3/2
5 1 3/2
5 1 1/2
5 0 1/2
4 3 7/2
4 3 5/2
4 2 5/2
4 2 3/2
4 1 3/2
4 1 1/2
4 0 1/2
3 2 5/2
3 2 3/2
3 1 3/2
3 1 1/2
3 0 1/2
2 1 3/2
2 1 1/2
2 0 1/2
ℓ 2 1 η 6 5 2 7 5 1 7 1 4 3 10 9 1 V 8 6 2 3 11 4 4'
F3ℓ F3α F3β F2β F1β F2γ1 F2γc F1γc
XBL747-5864

Fig. 12

P_{L_2}, and P_{L_3} which are the probabilities per α particle of shake-off in the L_1, L_2, and L_3 subshells respectively

$$P_{L_\alpha} = \left[P_{L_3} + P_{L_2} f_{23} + P_{L_1}(f_{13}+f_{12}\ f_{23})\right]\ \omega_3 F_{3\alpha} \tag{1}$$

$$P_{L_\beta} = \left[P_{L_3} + P_{L_2} f_{23} + P_{L_1}(f_{13}+f_{12}\ f_{23})\right]\ \omega_3 F_{3\beta} + (P_{L_2} + P_{L_1} f_{12})\ \omega_2 F_{2\beta} + P_{L_1}\ \omega_1 F_{1\beta} \tag{2}$$

$$P_{L_\gamma} = (P_{L_2} + P_{L_1} f_{12})\ \omega_2 F_{2\gamma} + P_{L_1}\ \omega_1 F_{1\gamma} \tag{3}$$

$$P_{L_\ell} = \left[(P_{L_3} + P_{L_2} f_{23} + P_{L_1}(f_{13}+f_{12}\ f_{23})\right]\ \omega_3 F_{3\ell} \tag{4}$$

The experimental resolution of the L x-rays was sufficient to resolve L_γ into $L_{\gamma 1}$ and $L_{\gamma c}$ (see Fig. 12) and their probabilities can be expressed as

$$P_{L_{\gamma 1}} = (P_{L_1} f_{12}+P_{L_2})\ \omega_2 F_{2\gamma 1} \tag{5}$$

$$P_{L_{\gamma c}} = (P_{L_1} f_{12}+P_{L_2})\ \omega_2 F_{2\gamma c} + P_{L_1}\omega_1 F_{1\gamma c} \tag{6}$$

also, $P_{L_{\beta 1,2}}$ and $P_{L_{\beta 4}}$ can be expressed as

$$P_{L_{\beta 1,2}} = \left[P_{L_3} + P_{L_2} f_{23} + P_{L_1}(f_{13}+f_{12}\ f_{23})\right]\ \omega_3 F_{3\beta 2} + (P_{L_2} + P_{L_1} f_{12})\ \omega_2 F_{2\beta 1} \tag{7}$$

$$P_{L_{\beta 4}} = P_{L_1} \omega_1 F_{1\beta 4} \tag{8}$$

where f_{12}, f_{13} and f_{23} are the values of the Coster Kronig yields and ω_1, ω_2 and ω_3 are the values of the subshell fluorescense yields. Their values are: $\omega_1 = 0.08 \pm 0.02$, $\omega_2 = 0.363 \pm 0.015$, $\omega_3 = 0.315 \pm 0.013$, $f_{12} = 0.15 \pm 0.04$, $f_{13} = 0.57 \pm 0.03$ and $f_{23} = 0.164 \pm 0.016$. F_{ij} represent the fraction of radiative transitions in the L_j peak connected with filling a vacancy in the L_i subshell. Thus, for example

$$F_{1\beta} = \frac{\sum \Gamma_{1\beta}}{\Gamma_1}$$

$$= \frac{\text{Intensity of L x-rays originating from } L_1 \text{ vacancies}}{\text{Total intensity of x-rays originating in } L_1 \text{ vacancies}}$$

$$= \frac{\Gamma(L_{\beta 4}) + \Gamma(L_{\beta 3}) + \Gamma(L_{\beta 10}) + \Gamma(L_{\beta 9})}{\Gamma_1}$$

Two sets of radiative rates were used. One was the set calculated by Scofield[43], and the other is an experimental set tabulated by Salem and Schultz[44]. Since Salem and Schultz listed only the major transitions (> 90%) their total values were normalized to Scofield's for the same transitions. From the L x-ray singles spectrum in the present work the ratio $F_{1\beta}/F_{1\gamma 2,3}$ agreed better with that determined from Salem and Schultz's list than Scofield's. I therefore believe the treatment using the former is the more accurate. Table I lists the values of F_{ij} used.

The probabilities P_{L_1}, P_{L_2} and P_{L_3} were calculated (see Table II) by two different methods. In method I Eqs. (5) and (6), which are linearly independent, are easily solved for P_{L_1} and P_{L_2}. Then, from Eq. (1) P_{L_3} is calculated. In this method only the data obtained in the coincidence run is used. The errors are calculated by assuming a maximum uncertainty of 10% in resolving L_γ into $L_{\gamma 1}$ and $L_{\gamma c}$ and do not include any errors in the C.K. coefficients, ω or F_{ij}. The consistency of the calculation is checked by determining P_{L_β} from Eq. (2) and the resulting value, $.99 \times 10^{-4}$ agrees with the experimental value, $.97 \times 10^{-4}$. In method II the values of $P_{L_{\beta 1,2}}$ and $P_{L_{\beta 4}}$ are obtained from the x-ray singles spectrum. Equation (8) is solved for P_{L_1}, and then Eqs. (7) and (1) are solved for P_{L_2} and P_{L_3}. With an assumption of 5% uncertainty in the determination of the ratio $P_{L_{\beta 4}}/P_{L_\beta}$, errors were calculated in the same way as for method I. With these calculated probabilities the abundance of P_{L_γ} as determined from Eq. (3), $.21 \times 10^{-4}$, agrees well with the experimental value $.22 \times 10^{-4}$. The results obtained in the two different methods also agree well with each other as shown in Table II, but method II gives more precise results and therefore the best values.

The total L shell ionization probability per α particle $P_L = P_{L_1}+P_{L_2}+P_{L_3}$ is listed in Table II. Also listed, is the total photon yield per α particle, P_{L_x}, which was determined from the equation:

$$P_{L_x} = P_{L_1}\left[\omega_1+f_{12}\omega_2+(f_{13}+f_{12}f_{23})\omega_3\right] + P_{L_2}(\omega_2+f_{23}\omega_3)+P_{L_3}\omega_3 \quad (9)$$

Table I. Normalized Salem and Schultz F_{ij} values

ij	F_{ij}
3α	0.760
3β	0.208
3ℓ	0.0336
2γ	0.201
2β	0.774
1γ	0.274
1β	0.693
2γ1	0.172
2γc	0.0286
1γc	0.274
1β4	0.292
2β1	0.773
3β2	0.172

The sensitivity of the calculated subshell shake-off probabilities to the parameters, ω and f, was also considered. The variation in f_{13} and f_{23} within the published errors result in the maximum changes of only 1 and 4% respectively in the ratio P_{L_2}/P_{L_3}. However, the possible variations in the other parameters result in a much more pronounced change as can be seen in Fig. 13(a-f). Variations in more than one parameter at a time could result in even larger changes than indicated. It is evident that more precise experimental or theoretical values of the input parameters are desirable.

2. M X-Rays

Figure 9 shows the photon radiation between 1.4 KeV and 4.7 KeV in coincidence with ^{210}Po α particles. K and Si x-rays which were obtained by exciting KBr and Si sources with ^{55}Fe radiation, served as energy and peak calibration standards. Silicon K x-rays excited in the α detector during the coincidence measurement were scattered into the x-ray detector and these also served as an internal calibration. In the x-ray singles spectrum the α detector was masked by a nickel foil and Si x-rays were not observed.

The M x-ray coincidence spectrum was resolved into its three major components: $M_\alpha(M_5\text{-}N_{6,7})$, $M_\beta(M_4\text{-}N_6)$ and $M_\gamma(M_3\text{-}N_5)$. The line $M_3\text{-}N_4$ was also included in M_γ. The abundances of the three components were determined as well as an upper limit on the number of counts registered in the $M_2\text{-}N_4$ peak. After correcting for the x-ray detector efficiency the abundances of M_α, M_β, M_γ and $M_2\text{-}N_4$ x-rays become

Table II. L Subshell Electron Shake-Off Probabilities

Shells	Probabilities x 10^4	
	I*	II**
P_{L_1}	4.92 ± .64	5.11 ± .60
P_{L_2}	.73 ± .24	.62 ± .06
P_{L_3}	1.60 ± .30	1.50 ± .19
P_L	7.25 ±1.18	7.23 ± .65
P_{L_x}	2.39 ± .39	2.37 ± .21

* Method I with Salem and Schultz's F_{ij}

** Method II with Salem and Schultz's F_{ij}

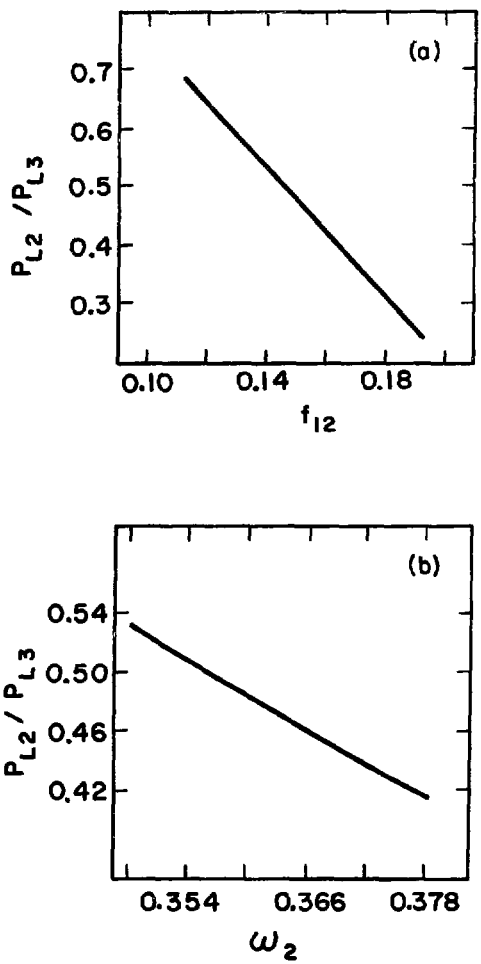
(a)
0.7
0.6
0.5
0.4
0.3
P_{L2}/P_{L3}
0.10
0.14
0.18
f_{12}
(b)
0.54
0.50
0.46
0.42
P_{L2}/P_{L3}
0.354
0.366
0.378
ω_2
XBL747-3662

Fig. 13 (a,b)

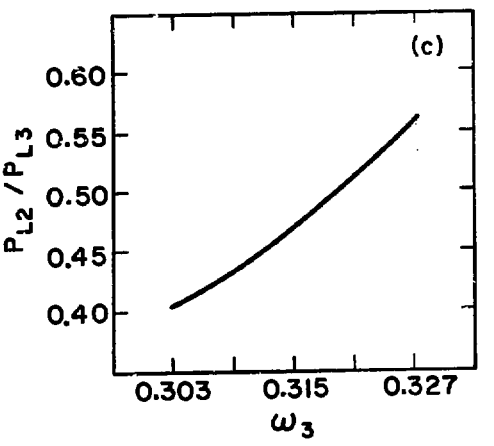

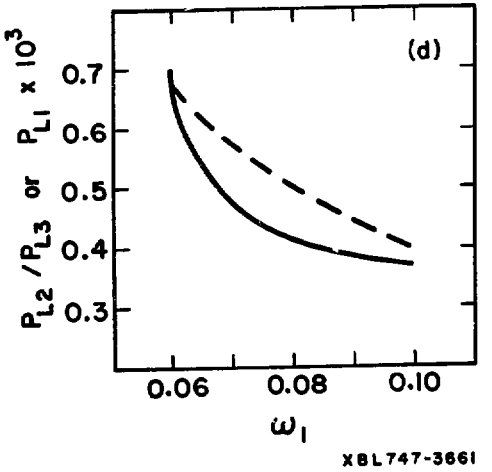

XBL747-3661

Fig. 13 (c,d)

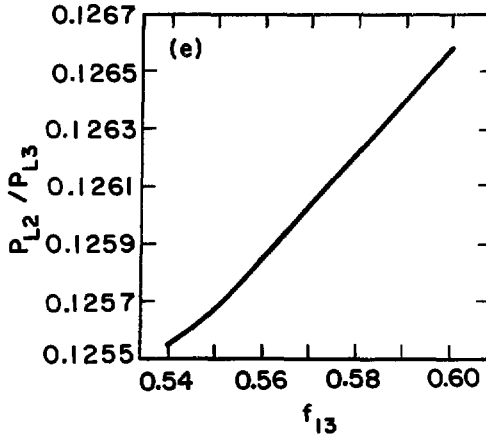

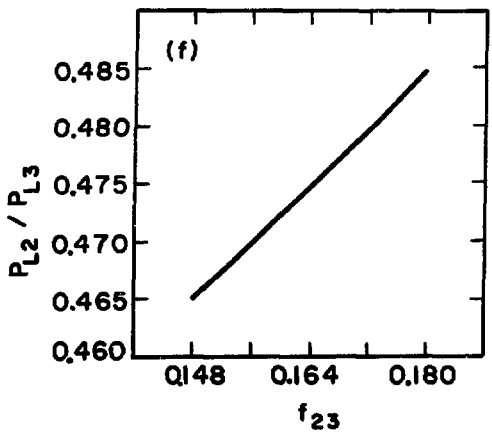

XBL747-3360

Fig. 13 (e,f)

$(2.9 \pm 0.6) \times 10^{-4}$, $(1.5 \pm 0.3) \times 10^{-4}$, $(0.78 \pm 0.16) \times 10^{-4}$, and $< 0.18 \times 10^{-4}$ respectively. The ratios of the line intensities are $M_\alpha:M_\beta:M_\gamma:M_2\text{-}N_4 = 100:52:27:<5$. These agree roughly with previous values[27] 100:66.6:33.3:10.

Figure 10 shows the corresponding M x-ray singles spectrum. Unfortunately, as was established after the experimental work was completed, intense chlorine K x-ray peaks masked part of the lead M x-ray energy region. X-ray fluorescence analyses of the same kind of beryllium foil as used for the ^{210}Po source backing plate, showed large amounts of the Cl x-ray peaks. The chlorine possibly arises from trichloroethane which is used sometimes to rinse beryllium after it is machined. A low energy x-ray spectrum of ^{241}Am deposited on the same type of foil showed that Cl x-rays were roughly proportional to the alpha activity of the source and indicated that less than 1% of the M peak observed in the ^{210}Po coincidence experiment was due to Cl x-rays. The $M_{\zeta 1}$ peak ($M_5\text{-}N_3$), which was masked by Si x-rays in the coincidence experiment, is not affected in the singles measurement because of a Ni shield in front of the α detector. Its abundance is $(0.23 \pm 0.05) \times 10^{-4}$ and the ratio $M_\alpha:M_{\zeta 1}$ is 100:8. This ratio agrees roughly with that deduced from the calculated[45] radiative transition probabilities, 100:3.5 but is in considerable disagreement with the ratio[27] 100:55.

From the coincidence counting rate, the average x-ray detector efficiency in the M x-ray region and the α singles counting rate, the photon yeild per α particle, P_{M_x}, was calculated to be $(5.52 \pm 1.10) \times 10^{-4}$.

With an average fluorescence yield, $\bar{\omega}_M$ = .03, the total M shell ionization probability per α particle is P_M= (1.84 ± .37) x 10^{-2} excluding the uncertainty in the average fluorescence yield. The large error associated with the above results is mostly due to the large uncertainty (10%) involved with the intensity of Np M x-rays that were used in the efficiency calibration of the x-ray detector.

Equations similar to the one written for L x-rays above can be written for the M x-rays

$$P_{M_\gamma} = P^*_{M_3}\omega_3 F_{3\gamma} \tag{10}$$

$$P_{M_\beta} = (P^*_{M_3} f_{34} + P^*_{M_4})\omega_4 F_{4\beta} \tag{11}$$

$$P_{M_\alpha} = \left[(P^*_{M_3} f_{34} + P^*_{M_4}) f_{45} + P^*_{M_3} f_{35} + P^*_{M_5} \right] \omega_5 F_{5\alpha} \tag{12}$$

where

$$P^*_{M_3} = P_{M_3} + P_{M_2} f_{23} + P_{M_1} (f_{13} + f_{12}\, f_{23})$$

$$P^*_{M_4} = P_{M_4} + P_{M_2} f_{24} + P_{M_1} (f_{14} + f_{12}\, f_{24})$$

$$P^*_{M_5} = P_{M_5} + P_{M_2} f_{25} + P_{M_1} (f_{15} + f_{12}\, f_{25})$$

but, the experimental data will not suffice to obtain unique results for the subshell ionization probabilities. However, from this type of analysis it is possible to determine several limits on the ionization

probabilities, e.g. $P_{M_2} = 7 - 23\%$; $P_{M_4} < 24\%$; $P_{M_5} < 17\%$; $P_{M_5} + P_{M_2} f_{25} < 17\%$; $P_{M_4} + P_{M_2} f_{24} < 28\%$; and $P_{M_1} + P_{M_3} > 47\%$ of the total. The input parameters used were taken from references 10 and 13 and an error of 10% was assumed in their value and in the relative values of the intensities of the M x-ray peaks.

3. α spectra

Figure 11 (a-e) presents the spectra of 8 days of experiment of ^{210}Po α particles in coincidence with x-rays. The coincidences in Fig. 11 (d) are due to α particles in coincidence with silicon K x-rays as discussed in the M x-ray section. This peak established the channel number that corresponded to ^{210}Po α_o particles and was later used as a standard peak shape in the coincidence run. The three spectra in Fig. 11 (a-c) are due to α particles in coincidence with lead L_α, L_β and L_γ x-rays. The peaks are labeled $\alpha_{L_\alpha,0}$, $\alpha_{L_\beta,0}$, $\alpha_{L_\gamma,0}$ as suggested in the section on the K shell effect. Also drawn into each spectrum is the peak shape that would have been expected to be observed if the ejected electrons carried-off zero kinetic energy and the initial vacancy distribution is as in Table II (second column). A similar plot for the α particles in coincidence with M x-rays is presented in Fig. 11 (e). The following remarks can be made: (1) As mentioned earlier the number of accidental coincidences was insignificant and no accidental α peak is observed in Fig. 11 (a-c). (2) The peaks due to L_α, L_β and L_γ are located 12.6 ± 1.4, 13.8 ± 1.4 and 17.6 ± 2.1 KeV lower than α_o in good agreement with their expected position (the binding energies of

L_3, L_2 and L_1 electrons are 13.035, 15.200 and 15.861 KeV respectively). (3) The peak due to M x-rays is located 3.1 ± 1.0 KeV lower than α_o which is in good agreement with the M binding energies of 2.5 to 3.9 KeV. (4) The peaks due to L vacancies are broader than the one due to M vacancies which in turn are only very slightly broader than the standard α peak. Also, every peak has a long tail on the lower energy side.

IV. *THEORY AND DISCUSSION*

The shake-off phenomenon accompanying α decay was treated by Migdal[1] as an example of adiabatic perturbation of the atomic cloud since the velocities of the α particles are much smaller than the velocities of the inner shell electrons. According to Migdal the perturbing potential is given by $V = -2\left[x^2 + y^2 + (z-vt)^2\right]^{-1/2}$. Here the alpha particle moves with velocity v along the positive z axis. Levinger[3] modified the perturbing potential by including the effect of the recoiling daughter nucleus (i.e. added to the above potential the term: $(Z-2)\left[x^2 + y^2 + (z+v_n t)^2\right]^{-1/2}$ where (Z-2) is the charge of the daughter nucleus which recoils with velocity v_n) which reduced the ionization probability of a K shell electron by a factor of ∿ 25. The latter probability is in total disagreement with experiment. However as was shown later[19,23], this modification is incorrect.

The ionization probabilities of inner shell electrons as calculated by the above two authors is given by asymptotic expansions. Migdal calculated only the first terms (dipole terms) of the expansions for the K, L and M electrons (see Ref. 1, Eq.(21)). In addition to his modification of the perturbing potential Levinger calculated also the second terms (quadrupole terms) of the expansions. He neglected the recoil effect in the quadrupole term since its contribution to that term was very small; hense recalculated the shake-off probabilities for K and L electrons only (see Ref. 3: Table IV corrected as noted by author). When the recoil cointribution to the ionization probabilities is factored out, Levinger's results of the calculation of the dipole

term are identical to Migdal's.

In the above calculations the bound electrons and the electrons ejected into the continuum are described by non-relativistic hydrogenic type wave functions. A more realistic set of wave functions would be of the self consistent type. In the following paragraphs, the details of Migdal's treatment with the latter type of wave functions of the K shell ionization accompanying α decay are described.:

According to Migdal the probability of ionizing one of the 1s electrons is given by:

$$dP_{1s} = \frac{8v^2}{3(E_k - B)} \left| < K, \ell=1 \left| \frac{1}{r^2} \right| 1s > \right|^2 dE_k \qquad (13)$$

+ much smaller terms

where v is the velocity of the α particle, B is the binding energy of a 1s electron and E_k is kinetic energy carried off by the ionized 1s electron. The matrix element can be readily calculated with hydrogenic wave functions and the probability equation becomes:

$$dP_{1s} = \frac{2^{11} v^2}{3 \cdot Z^6} \frac{e^{-\frac{4Z}{k} \text{Arctan } k/Z}}{\left(1 + \frac{k^2}{Z^2}\right)^5 \left(1 - e^{-2\pi Z/k}\right)} dE_k \qquad (14)$$

where Z is the charge of the daughter nucleus and $k = \sqrt{2E_k}$. One gets the total ionization probability by numerical integration.

The hydrogenic type wave functions used in Eq. (13) were replaced by Hartree-Fock-Slater wave functions (H-F-S). For the bound 1s electrons use was made of H-F-S radial wave functions that are already tabulated.[46] The continuum-electron radial wave functions, $P_{k\ell}$

(described by the wave vector k and the angular momentum ℓ), were determined by numerically solving the radial equation

$$\left(\frac{d^2}{dr^2} - \frac{\ell(\ell+1)}{r^2} - 2\left[E_k - V(r)\right]\right) \quad P_{k\ell}(r) = 0 \tag{15}$$

The potential V(r) was the tabulated[46] H-F-S central potential that was developed in the H-F-S solution for the bound electrons. The Numerov[47] integration method was applied until the solution became asymptotic. The two points at small r required to generate the solutions were taken to be hydrogenic. The asymptotic solution is known to be[48]

$$P_{k\ell}(r) \approx \left(\frac{2}{\pi k}\right)^{1/2} \cos\left[kr + k^{-1}\ln(2\,kr) - \frac{1}{2}\pi(\ell+1) - \delta_\ell\right] \tag{16}$$

where $\delta_\ell = \arg\ \Gamma(\ell+1+i\frac{z}{k})$ is the complex phase of the Γ-function. Using the derivative of Eq. (16) one can write

$$P^2_{k\ell}(r) + \frac{P'^2_{k\ell}(r)}{\left(k+\frac{1}{kr}\right)^2} = \frac{2}{\pi k} \tag{17}$$

Equation (17) is independent of r for large r. Thus, the numerical solution for the continuum wave function can be normalized by requiring Eq. (17) to hold for large r. With these solutions and the tabulated[46] ls wave functions the matrix elements in Eq. (13) were calculated and the probability *vs.* energy relation was obtained. The total probability was obtained by numerical integration.

Table III lists the values of the matrix elements calcualted for ^{210}Pu as a function of the kinetic energy carried off by the

ionized 1s electron. The energy distribution calculated from Eq. (13) with H-F-S type wave functions are almost identical with those calculated with the hydrogenic type (see Eq. (14)).

Using the calculations of shake-off probability as a function of electron energy and the experimental average peak shape in the ^{210}Po α singles spectrum the shape of the α spectrum associated with the shake-off of K electrons which would be expected from Migdal's theory was determined. The theoretical shape was normalized to the same peak height as the experimental curve and is shown as a dashed line in Fig. 7. The α singles spectrum had a small perturbation about 300 KeV below the peak due to instrumental effects and this is reflected in both the calculations and the coincidence spectrum. As seen in Fig. 7, there is a definite discrepancy between the experimental and theoretical curves. The probability of electron shake-off decreases more rapidly than the theoretical prediction as the electron energy increases (i.e., as the α particle energy decreases). Ovechkin and Tsenter[23] observed the same effect in comparing electron energy measurements with Migdal's calculations, but the authors felt their experimental work was not sufficiently precise to indicate a definite decrepancy.

The total probability of electron (see Table IV) shake-off from the K shell was calcualted from Eqs. (13) and (14). In Eq. (14), Z the charge of the daughter nucleus was replaced by the effective charge Z^*; Z^*(uranium) = 91.26 and Z^*(lead) = 81.27. Here, v (α particle)/ v(1s electron) is 0.0817 for uranium and 0.0899 for lead.

Table III. Matrix Element (Eq. 13) as a Function of Electron Energy

Energy*	$< > \times 10^{-1}$		Energy	$> \times 10^{-1}$		Energy	$< > \times 10^{-1}$	
	a	b		a	b		a	b
1.	4.2972	4.8347	400.	4.4003	4.9254	1700.	4.6223	5.1367
10.	4.3004	4.8375	500.	4.4226	4.9454	1800.	4.6346	5.1493
20.	4.3038	4.8406	600.	4.4438	4.9647	1900.	4.6464	5.1615
30.	4.3056	4.8435	700.	4.4641	4.9833	2000.	4.6577	5.1733
40.	4.3089	4.8455	800.	4.4834	5.0013	2100.	4.6685	5.1846
50.	4.3114	4.8473	900.	4.5018	5.0187	2200.	4.6790	5.1956
60.	4.3140	4.8491	1000.	4.5194	5.0354	2300.	4.6889	5.2063
70.	4.3169	4.8511	1100.	4.5361	5.0514	2400.	4.6986	5.2166
80.	4.3199	4.8533	1200.	4.5521	5.0669	2500.	4.7078	5.2266
90.	4.3228	4.8556	1300.	4.5675	5.0819	2600.	4.7166	5.2363
100	4.3256	4.8589	1400.	4.5821	5.0963	2700.	4.7251	5.2457
200.	4.3529	4.8823	1500.	4.5961	5.1103	2800.	4.7333	5.2548
300.	4.3770	4.9046	1600.	4.6095	5.1237	2900.	4.7412	5.2636

(continued)

Table III. (continued)

Energy*	< > x 10^{-1}		Energy	< > x 10^{-1}		Energy	< > x 10^{-1}	
	a	b		a	b		a	b
3000.	4.7488	5.2722	8000.	4.9188	5.4948	13200.	4.9321	5.5390
3200.	4.7631	5.2885	8400.	4.9229	5.5022	13600.	4.9307	5.5392
3600.	4.7887	5.3185	8800.	4.9263	5.5086	14000.	4.9291	5.5392
4000.	4.8107	5.3451	9200.	4.9291	5.5143	14400.	4.9273	5.5390
4400.	4.8299	5.3688	9600.	4.9313	5.5193	14800.	4.9254	5.5386
4800.	4.8464	5.3900	10000.	4.9329	5.5234	15200.	4.9233	5.5379
5200.	4.8607	5.4089	10400.	4.9341	5.5271	15600.	4.9210	5.5371
5600.	4.8731	5.4258	10800.	4.9348	5.5301	16000.	4.9186	5.5361
6000.	4.8839	5.4409	11200.	4.9352	5.5326	16400.	4.9161	5.5349
6400.	4.8931	5.4543	11600.	4.9351	5.5347	16800.	4.9135	5.5336
6800.	4.9012	5.4663	12000.	4.9348	5.5363	17200.	4.9107	5.5323
7200.	4.9080	5.4769	12400.	4.9342	5.5375	17600.	4.9079	5.5308
7600.	4.9138	5.4864	12800.	4.9333	5.5384	18000.	4.9049	5.5292

*Energy in atomic units; 1 a.u. = 27.21 eV.

a - ^{210}Po.

b - ^{238}Pu.

Table IV. Probability of Electron Shake-Off From the K Shell

Isotope	Ref.	Experiment	Stated Error	Theory (Hydrogenic)	Theory (H-P-S)	Hansen[19]
^{210}Po	24	1.5×10^{-6}	± 33%			
	25	2.0	± 16%			
	25	1.6	± 31%			
	20	1.5	± 27%			
	This work	1.65	± 10%	2.67×10^{-6}	2.87×10^{-6}	2.02×10^{-6}
^{238}Pu	15	0.51	± 50%			
	This work	0.75	± 12%	1.75×10^{-6}	1.66×10^{-6}	

Recently, Hansen[19] in a different type of theoretical treatment calculated the shake-off probabilities of K, L and M electrons. In his treatment, the above probabilities were described as special zero-impact-parameter trajectories in the generalized impact-parameter formulation of a binary encounter approximation. Hansen had taken into account two additional effects not accounted for in Migdal's theory: relativistic effects and the variation of the kinetic energy of the α particle in the vicinity of the nucleus. His result, 2.02×10^{-6} is somewhat closer in agreement with the experimental result than any of the theoretical values. Unfortunately the shake-off probability as a function of electron energy was not calculated by Hansen. Table IV summarized the experimental results and the theoretical results on the shake-off effect in the K shell accompanying α decay.

In Table V the experimental work on L and M electron shake-off up to date is summarized and compared with theoretical predictions. The following values of the effective charge were used: $Z^*(2s) = 77.34$, $Z^*(2p) = 76.23$, $Z^*(3s) = 69.28$, $Z^*(3p) = 67.33$ and $Z^*(3d) = 64.81$. Here the values of alpha particle velocity over electron velocities are 0.189, 0.192, 0.316, 0.325 and 0.338 for 2s, 2p, 3s, 3p and 3d electrons respectively.

The L subshells ionization probabilities as listed by Migdal and Levinger are all smaller than the probabilities calculated from the experiment and the theoretical series expansion converges rather slowly. These suggest the need to calculate additional terms in the expansion. Also, a more realistic set of wave function, relativistic

Table V. Probability of Electron Shake-Off From the L and M Shells

Shell		Theory		Experiment**	Ref.
		Migdal[1]	Hansen[19]		
	D*	4.300×10^{-5}			
	Q*	0.002×10^{-5}			
P_{L_1}	Total	4.302×10^{-5}	2.30×10^{-4}	$(5.11 \pm 0.40)\times10^{-4}$	This work
	D	2.791×10^{-5}			
	Q	0.0889×10^{-5}			
P_{L_2}	Total	3.680×10^{-5}	0.76×10^{-4}	$(0.62 \pm 0.06)\times10^{-4}$	This work
	D	5.582×10^{-5}			
	Q	2.525×10^{-5}			
P_{L_3}	Total	8.107×10^{-5}	2.86×10^{-4}	$(1.50 \pm 0.19)\times10^{-4}$	This work
P_L		1.61×10^{-4}	5.9×10^{-4}	$(7.23 \pm 0.65)\times10^{-4}$	This work
P_{L_x}		0.54×10^{-4}	1.83×10^{-4}	$(2.2 \pm 0.5)\times10^{-4}$	3
				$(2.93 \pm 0.43)\times10^{-4}$	4
				$(2.79 \pm 0.42)\times10^{-4}$	5
				4×10^{-4}	2
				$(2.37 \pm 0.21)\times10^{-4}$	This work
P_M		1.67×10^{-3}†	1.90×10^{-2}	$(1.84 \pm 0.37)\times10^{-2}$	This work
P_{M_x}		5.01×10^{-5}†	5.7×10^{-4}	$(5.52 \pm 1.10)\times10^{-4}$	This work
				1.5×10^{-3}	2
				0.91×10^{-3}	5

* D = Dipole term, Q = Quadrupole term

** The errors in the present work do not include uncertainties in the values of ω, f and F_{ij}.

† Dipole term only.

Hartree-Fock wave functions for example, should be used in the calculations rather than hydrogenic type wave functions. Similar remarks can be made with regard to M shell shake-off calculations.

Hansen's calculations for the L and M shells are in far better agreement with experimental result than Migdal's theory. His photon yields agree well with experiment. However, the agreement is not good for the individual L subshell ionization probabilities. However, this is not reflected in the photon yield since the latter is not very sensitive to the initial subshell vacancy distribution. It will be interesting to compare the differential shape of the α spectrum with the differential shape that Hansen's treatment will predict and is yet to be calculated.

In addition to comparing experimental shake-off probabilities with theoretical predictions, the former could be compared with experimental ionization of lead by 5.3 MeV α particle bombardment. Unfortunately measurements at this energy have not been reported. Available[49] are Pb L subshell ionization cross-section ratios vs proton bombarding energy from 0.5 to 4 MeV. Also reported[50] are cross-sections for L subshell ionization in Au by collision of protons (0.25 - 5.2 MeV) and α particles (1 - 12 MeV). The latter measurements show that for energies greater than ∿1.4 MeV/nucleon the L subshell ionization cross-scetion ratios for proton bombardment are very similar to the ratios for α particle bombardment. Therefore a good estimate of lead ionization cross-section

ratios by 5.3 MeV (1.32 MeV/nucleon) α particles was obtained from reference 49. These are: $\sigma_{L_2}/\sigma_{L_1} \approx 3.2$ and $\sigma_{L_3}/\sigma_{L_2} \approx 4.0$. The ionization probability ratios due to shake-off effect are: $P_{L_2}/P_{L_1} = 0.12$ and $P_{L_3}/P_{L_2} = 2.4$. Thus, $\sigma_{L_3} > \sigma_{L_2} > \sigma_{L_1}$ while $P_{L_1} > P_{L_3} > P_{L_2}$.

V. SUMMARY AND CONCLUSION

Most of the new information presented in this paper concerns the direct observation of that part of the alpha spectrum connected with the electron shake-off effect in the K, L and M shells. These peaks, $\alpha_{K,0}$ and $\alpha_{K,44}$ in the decay of ^{238}Pu and $\alpha_{K,0}$, $\alpha_{L_\gamma,0}$, $\alpha_{L_\beta,0}$, $\alpha_{L_\gamma,0}$ and $\alpha_{M,0}$ in the decay of ^{210}Po, were experimentally observed for the first time. As conservation of energy required the energy differences between α_0 in ^{210}Po and ^{238}Pu and α_{44} in ^{238}Pu, and their corresponding α shake-off peaks were equal to the binding energies of the ionized electrons. The shape of the α spectra indicated that part of the latter were ejected with kinetic energy greater than zero.

It is clear that Migdal's theory still predicts ionization probabilities of K electrons approximately twice as high as observed experimentally. The use of H-F-S type wave functions has little effect on the total ionization probabilities. Also, the energy distributions calculated with H-F-S type wave functions are almost identical with those calculated with the hydrogenic type. The theoretical energy distribution of the ejected electrons does not fall as rapidly with increasing energy as the experimental one.

It is possible the discrepancies mentioned above could be reduced by using relativistic Hartree-Fock wave functions. These wave functions should be made very accurate at small distances since this is the region where most of the strength of the matrix elements lies. An experimental study of ^{148}Gd similar to the ones presented

in this paper should indicate if Migdal's theory gives the proper dependence on both charge and alpha particle energy.

For better comparison between Migdal's theory and the shake-off phenomena in the L and M shells it is necessary to calculate additional terms in the asymptotic expansion.

Hansen's new theoretical treatment predicts ionization probabilities in closer agreement with experiment than Migdal's. However, discrepancies still exist. Also energy distributions for the ejected electrons were not calculated. It is clear that more experimental investigations of L and M shell electrons is needed. The analysis of these experiments will be more complicated due to the presence of L and M x-rays that originate in the internal conversion process. Measurements of the abundance of N shell effect, which should be substantially larger than that in the M shell, could indicate what would be the "best" alpha peak shape or resolution which present-day high-resolution α spectrometers could obtain.

REFERENCES

1. A. Migdal, J. Phys. (USSR) 4, 449 (1941).
2. E. L. Feinberg, J. Phys. (USSR) 4, 423 (1941).
3. J. S. Levinger, Phys. Rev. 90, 11 (1953); J. Phys. Rad. 16, 556 (1955).
4. T. A. Carlson, C. W. Nestor, Jr., T. C. Tucker, and F. B. Malik, Phys. Rev. 169, 27 (1968).
5. A. J. Mord, Nucl. Phys. A192, 305 (1972).
6. J. Law and J. L. Campbell, Nucl. Phys. A185, 529 (1971); Nucl. Phys. A187, 525 (1972); Nucl. Phys. A199, 481 (1973).
7. T. Mukoyama, Y. Isozumi, T. Kitahara, and S. Shimizu, Phys. Rev. C 8, 1308 (1973).
8. R. L. Intemann, Nucl. Phys. A219, 20 (1974).
9. T. Mukoyama, T. Kitahara, and S. Shimizu, Phys. Rev. C 9, 2307 (1974).
10. T. Mukoyama, and S. Shimizu, Phys. Rev. C 9, 2300 (1974).
11. C. W. E. Van Eijk and T. W. Kooy, Phys. Letters 46B, 351 (1973).
12. J. L. Campbell and J. Law, Can. J. Phys. 50, 2451 (1972).
13. Y. Isozumi and S. Shimizu, Phys. Rev. C 4, 522 (1971).
14. E. der Mateosian, Phys. Rev. A 3, 573 (1971).
15. H. J. Nagy, G. Schupp, and R. R. Hurst, Phys. Rev. C 6, 607 (1972).
16. A. Bond, O.P. Gupta, and A. Zide, Phys. Rev. C 9, 1529 (1974).
17. C. W. E. Van Eijk, R. W. Kooy, and M. J. C. Visscher, Phys. Rev. C 9, 2074 (1974).
18. F. T. Porter, M. S. Freedmann, and F. Wagner,Jr., Phys. Rev. C 3, 2246 (1971).

19. J. S. Hansen, Phys. Rev. A 9, 40 (1974).

20. M. A. Grace, R. A. Allen, D. West, and H. Halban, Proc. Phys. Soc. (London) A64 , 493 (1951).

21. W. C. Barber and R. H. Helm, Phys. Rev. 86, 275 (1952).

22. M. Riou, J. Phys. Rad. 13, 487 (1952).

23. V. V. Ovechkin and E. M. Tsenter, Soviet J. At. Energy, English Transl. 2, 344 (1957).

24. I. Curie and F. Joliot, J. Phys. Rad. 7, 20 (1931).

25. M. Riou, J. Phys. Rad. 13, 487 (1952).

26. W. Rubinson and W. Bernstrin, Phys. Rev. 86, 545 (1952).

27. W. Rubinson, Phys. Rev. 130, 2011 (1963).

28. C. M. Lederer, private communication.

29. S. Szucs and J. M. Delfoss?, Phys. Rev. Lett. 15, 163 (1965).

30. K. C. K. Günter, F. Asaro, and A. C. Helmholz, Phys. Rev. Lett. 16, 362 (1966).

31. G. L. Cano and R. W. Dressel, Phys. Rev. A139, 1883 (1965).

32. N. Perrin and W. de Wieclawick, C. R. Acad. Sc. 262, 511 (1966); C. R. Acad. Sc. 266, 577 (1968); C. R. Acad. Sc. 268, 1268 (1969).

33. J. Meyer, J. M. Paulus, and J. Ch. Abbe, Radiochimica Acta 17, 76 (1972).

34. G. C. Nestor, B. G. Sounders, and S. T. Salem, atomic data 1, 337 (1970).

35. J. S. Hansen, J. C. McGeorge, D. Nix, W.D. Schmidt - Ott, I. Unus and R. W. Fink, Nucl. Instr. and Meth. 106, 365 (1973).

36. J. Legrand, Nucl. Instr. and Meth. 112, 229 (1973).

37. J. L Campbell and L. A. McNelles, Nucl. Instr. and Meth. 98, 433 (1972).

38. D. A. Landis, C. F. Jones, B. V. Jarrett, A. Jue, and S. D. Wright, LBL-540, June 1972.

39. Unpublished

40. Nuclear Data Sheets B5/6, 648 (1971).

41. R. S. Hager and E. C. Seltzer, Nuclear Data Tables A4, 1 (1968).

42. W. Bambynek, B. Crasemann, R. W. Fink, H. U. Freund, H. Mark, C. D. Swift, R. E. Price and P. Venugopala Rao, Rev. Mod. Phys. 44, 716 (1972).

43. J. H. Scofield, Phys. Rev. 179, 9 (1969).

44. S. I. Salem and C. W. Schultz, Atomic Data 3, 215 (1971).

45. C. P. Bhalla, J. Phys. B 3, 916 (1970).

46. F. Herman and S. Skillman, Atomic Structure Calculations, Prentice-Hall, Inc. (1963).

47. J. M. Blatt, J. Comp. Phys. 1, 382 (1967).

48. H. Bethe and E. E. Salpeter, Quantum Mechanics of One and Two Electron Atoms, Academic, New York (1957).

49. D. H. Madison, A. B. Baskin, C. E. Busch, and S. M. Shaforth, Phys. Rev. A 9, 675 (1974).

50. S. Datz, J. L. Duggan, L. C. Feldman, E. Laegsgaard, and J. U. Anderson, Phys. Rev. A 9, 192 (1974).

FIGURE CAPTIONS

Fig. 1 Block diagram of electronics used for α - K x-ray coincidence measurements.

Fig. 2 ^{210}Po photon radiation between 20 KeV and 150 KeV.

Fig. 3 ^{238}Pu photon radiation between 35 KeV and 180 KeV.

Fig. 4 Block diagram of electronics used for α - L and M x-ray coincidence measurements.

Fig. 5 ^{238}Pu α spectrum in coincidence with uranium K_β x-rays.

Fig. 6 Partial decay scheme of ^{238}Pu.

Fig. 7 ^{210}Po α spectrum in coincidence with lead K_α x-rays. --- theoretical shape normalized to peak height.

Fig. 8 Lead L x-rays (8.37 eV/channel) in coincidence with ^{210}Po α particles.

Fig. 9 Lead M x-rays (8.37 eV/channel) in coincidence with ^{210}Po α particles.

Fig. 10 Lead M x-rays (8.37 eV/channel) singles spectrum.

Fig. 11 a,b,c ^{210}Po α spectrum (.85 KeV/channel) in coincidence with lead L_α, L_β and L_γ x-rays.

Fig. 11 d,e ^{210}Po coincidence α spectrum (.85 KeV/channel).

(d) ^{210}Po α spectrum in coincidence with solicon x-rays which scattered from α detector into x-ray detector.

(e) ^{210}Po α spectrum in coincidence with lead M x-rays.

Fig. 12 Spectroscopic diagram for the major radiative transitions that comprise the characteristic L x-rays spectrum.

Fig. 13 a,b Variation of deduced L subshell probabilities as function of f_{12} or ω_2.

Fig. 13 c,d Variation of deduced L subshell probabilities as function of ω_3 or ω_1.

Fig. 13 e,f Variation of deduced subshell probabilities as function of f_{13} or f_{23}.

ACKNOWLEDGMENTS

I am indebted to the Lawrence Berkeley Laboratory of the Univeristy of California and to the United States Atomic Energy Commission for the facilities and support required for this study.

These experiments relied heavily on properly functioning electronic equipment. I am grateful to Duane Mosier for making the experiments possible by providing his assistance and advice throughout this study.

I am grateful to Helen Michel for her patient tutelage and help with regard to the chemistry of the radioactive materials used in the experiment. I am also grateful to Eldren Calhoon of the Health Chemistry Division for providing assistance with all matters of handling and safety of radioactive materials.

I am grateful to my advisor, Professor Isadore Perlman, for suggesting the problem to be studied, and most important to Dr. Frank Asaro under whose supervision and constant advice this study was carried out.

Special thanks to my wife, Nili, for her interest in my work and her aid in the preparation of this manuscript.